Atomic transition probabilities and tests of the spectroscopic coupling scheme for N I

J. Musielok,* W. L. Wiese, and G. Veres†
National Institute of Standards and Technology, Gaithersburg, Maryland 20899
(Received 7 November 1994)

With a wall-stabilized arc source, we have measured the relative transition probabilities of 100 lines of neutral nitrogen in the visible and near-infrared spectrum and have normalized our data to an absolute scale utilizing four recent lifetime results. We estimate that the expanded uncertainties of our data are in the range of ±11–15 %. For a number of $3s$-$3p$ and $3p$-$3d$ multiplets, we have measured complete sets of lines and observe that most $3p$-$3d$ multiplets show considerable departure from *LS* coupling, while the $3s$-$3p$ multiplets adhere to it within ±20%. Agreement between intermediate coupling calculations and our experimental data for the $3p$-$3d$ multiplets is noticeably better, but significant differences are still encountered for two multiplets originating from the $3d\ ^4P$ level.

PACS number(s): 32.70.Cs, 32.90.+a

I. INTRODUCTION

During the last few years, two comprehensive sets of atomic transition probabilities for N I have been calculated with sophisticated atomic structure methods. They are the Opacity Project (OP) calculations by Burke and Lennon [1]—a frozen-core type configuration-interaction approximation based on a close-coupling approach in conjunction with the *R*-matrix method [2]—and the configuration interaction calculations by Hibbert *et al.* [3], carried out with the configuration-interaction version 3 (CIV3) code [4]. Furthermore, Weiss and Suskin [5] have carried out sophisticated calculations on a limited scale.

All three approaches [1,3,5] include extensive treatments of configuration interaction, a critical requirement in atomic structure calculations for all but the simplest atomic systems. These calculations are therefore expected to provide greatly improved sets of transition probabilities for this spectrum.

The OP data are multiplet values so that comparisons with this theory can be done on that level only. The CIV3 and the Weiss-Suskin calculations have been carried out for individual lines, and have been done in intermediate coupling by including Breit-Pauli relativistic interactions. Considerable departures from *LS* coupling—which usually prevails for light atoms—were obtained.

Experimental comparison material has been quite limited for this spectrum, so that these calculations have not been sensitively tested as yet, both for the multiplet values and for the individual lines. Emission experiments by Goldbach *et al.* [6] and Zhu *et al.* [7] (normalized to absolute scales based on lifetime measurements) have provided some experimental results which are in closer agreement with the work of Hibbert *et al.* [3] and with Weiss and Suskin [5] than with the OP results [1]. However, those particular multiplets are not especially sensitive to configuration interaction. Furthermore, the measurements as well as Hibbert *et al.*'s calculations are not far from *LS* coupling; larger departures from *LS* coupling as well as higher sensitivity to configuration interaction are expected for other types of multiplets, for example some $3p$-$3d$ transitions, which have not been studied in recent experiments. We have therefore experimentally investigated a number of multiplets where larger deviations are expected on account of the theoretical work by Hibbert *et al.*

We have generated a stable steady-state plasma with a wall-stabilized arc and measured relative transition probabilities of individual lines in various $3s$-$3p$, $3p$-$3d$, $3s$-$4p$, $3p$-$4d$, and $3p$-$5s$ multiplets, covering about 100 prominent lines in the visible and near-infrared regions of the spectrum. We also included some relatively strong intersystem lines in our measurements. Our data were placed on an absolute scale provided by recent lifetime data.

II. METHOD

This experiment has two distinctive parts: measurements of the strengths of the components, or spectral lines, in multiplets to test the coupling scheme, and measurements of the multiplet and line A values on an absolute, experimentally derived scale.

For the first part, we have measured the intensity ratios I_X/I_R of neutral nitrogen lines within multiplets. For each multiplet we have selected, somewhat arbitrarily, a relatively strong line as our reference line, R, and, have obtained transition probability ratios A_X/A_R for other lines labeled X versus the reference line via the relation [6,7]

$$\frac{A_X}{A_R}=\frac{I_X\lambda_X g_R}{I_R\lambda_R g_X}\exp\left[\frac{E_X-E_R}{kT}\right]. \tag{1}$$

A denotes the transition probability, g the statistical weight, and E the excitation energy of the *upper* level of

*Permanent address: Opole University, 45-052 Opole, Poland.
†Permanent address: KFKI Research Institute for Particle and Nuclear Physics, 1525 Budapest, Hungary.

 ©1995 The American Physical Society

the transition, λ the wavelength of the line, k the Boltzmann constant, and T the plasma temperature. E, λ, and g are very accurately known for all investigated lines [8], and the plasma temperature T has been experimentally determined (see below). Since we restrict ourselves to line ratios within multiplets, the upper (as well as lower) state quantum numbers of such lines are the same with respect to n, l, L, and S, but they differ in J. Atomic levels sharing the same set of quantum numbers except J are typically grouped very closely together in energy, differing by very small amounts only. In fact, some of the multiplet transitions even share the same upper energy levels. For the multiplets investigated here—mostly $3s$-$3p$ and $3p$-$3d$ transitions—the largest energy differences between the upper levels within the multiplets amount to about 0.1% of the excitation energies which are typically in the range of 12–14 eV. With an arc temperature kT of about 1 eV, the exponential term in Eq. (1) is therefore always very close to unity. However, even though it amounts to less than 1% in all cases we nevertheless include this term in our calculation of A ratios, utilizing our measurement of the arc temperature as described below.

Furthermore, since the wavelengths in multiplets are nearly the same for all lines, the intensity ratios according to Eq. (1) are essentially proportional to the gA ratios. Therefore, accurate intensity (radiance) measurements are the only critical requirement for obtaining reliable, accurate transition probability ratios within multiplets.

Since we measured complete sets of line intensity ratios in multiplets, we found it convenient to express line gA values as fractions of multiplet $g_M A_M$ values. By applying Eq. (1) to the ratio of a single line (L) to the whole multiplet (M), one obtains

$$g_L A_L = g_M A_M \frac{I_L \lambda_L}{I_M \lambda_M} \exp\left[\frac{E_L - E_M}{kT}\right] . \tag{2}$$

The multiplet intensity is the sum of the line intensities $I_M = \sum I_L$, and the multiplet values of E_M, g_M, and λ_M are given as [9]

$$E_M = (g_1 E_1 + g_2 E_2 + \cdots)/(g_1 + g_2 + \cdots) , \tag{3}$$

$$g_M = (2L+1)(2S+1) , \tag{4}$$

$$\lambda_M = hc(E_M^k - E_M^i)^{-1} . \tag{5}$$

In Eq. (4), L and S denote the orbital angular momentum and spin quantum numbers for the multiplet. Indices for lower and upper levels i and k, respectively, have been omitted in Eqs. (3) and (4), since this applies to both upper and lower levels (arbitrarily labeled 1,2,. . .) of the multiplet.

In the second part of the experiment, we have measured—with a somewhat different experimental approach but again utilizing Eq. (1)—transition probability ratios between strong lines from *different* multiplets (using $3s\ ^4P_{5/2}$–$3p\ ^4D^o_{7/2}$ as the reference line) in order to tie all multiplets together on a common relative scale. For these measurements, the determination of the temperature is important, since the excitation energies for different multiplets are significantly different. The relative scale is then converted to an absolute scale by normalizing the transition probabilities of lines originating from the $3p\ ^4D^o_{7/2}$ and $3p\ ^4S^o_{3/2}$ levels against recent lifetime measurements.

III. EXPERIMENT

The nitrogen spectra were studied with a high current wall-stabilized arc discharge [10]. The arc was operated in the center of a stack of seven water-cooled disks with a 4-mm-diam central bore. The 6.3-mm-thick disks were separated by relatively wide, 2-mm-thick insulating spacers. The electrodes consisted of water-cooled tungsten for the cathode and copper for the anode. The areas close to both electrodes were operated in argon gas, while the midsection of the arc channel (about 25% of its length) was operated in helium with a small addition of nitrogen, typically about 0.5% by volume. These conditions were achieved by a suitable arrangement of several gas inlet and exhaust openings along the arc channel and by appropriate adjustments of the gas flow rates. The arc was operated at a current of 50 A. The observations of individual line intensities in multiplets were carried out side-on, while the measurements of line intensity ratios involving different multiplets were done end-on, for reasons explained later.

Operating the arc source in helium produces appreciable populations of the excited N I levels at rather low electron densities. This feature yields two important advantages: (a) narrow lines, minimizing overlap in multiplets, and (b) fairly large line-to-continuum ratios, facilitating accurate intensity measurements even for weak lines. A special construction of the central arc section (disk) allowed the observation of the emitted radiation side-on from a volume element of full arc constriction and free of macroscopic electric fields along the arc axis. This section has the shape shown in Fig. 1. The disk has a narrow channel that runs through the center and has a diameter of 1.5 mm for the region close to the central bore that contains the plasma. This opening is widened to 4 mm at the halfway point to the outside walls. This construction provides a sufficiently large solid angle for

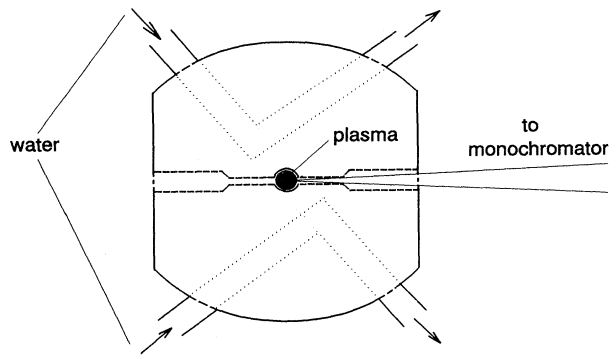

FIG. 1. Cross-sectional schematic view of the central arc disk.

spectral observations of the radiation emitted by the arc. Windows are normally attached to the side-on observation ports.

Figure 2 shows the schematic optical arrangement for the spectroscopic measurements. The concave mirror CM1 was located on the main optical axis defined by the 2-m Czerny-Turner monochromator. This concave mirror imaged either the arc or the radiometric standard source onto the entrance slit of the monochromator with a magnification factor of 1.3 via a rotating plane mirror $M1$ which was located slightly below the optical axis. The solid angle for all arc observations was $f/50$. The radiation emerging from the arc in the direction opposite to the Czerny-Turner monochromator was reflected back into the arc—when needed—by the concave mirror CM2 placed at a distance of twice its focal length from the arc. With this arrangement, self-absorption checks were performed [11]. Ratios could be obtained between signals (a) from the arc plus its reflected image and (b) from the arc only. These ratios were obtained on a point-by-point basis over the wavelength range of the studied lines by utilizing a mechanical shutter in front of CM2. Constant ratios everywhere over the range of the line profile indicated optically thin conditions. For the critical regions around the line centers these conditions could always be achieved by appropriate adjustments of the nitrogen amounts added to the helium carrier gas.

The radiation emitted in the direction opposite to the Czerny-Turner monochromator was also used to monitor the stability of the arc emission. For this purpose the concave mirror CM3 (see Fig. 2) collected some radiation at an angle slightly off the main optical axis and imaged the arc—via the plane mirror $M2$—onto the entrance slit of a 1/4 m grating monochromator. The emission of a N II line at 3995 Å, with a peak intensity about five times the underlying continuum level, was monitored during the measurements to determine the stability of the nitrogen emission. Fluctuations of this line intensity during the experimental runs were found to be within 1%.

As mentioned earlier, the measurements were performed in two parts. First, intensity ratios of individual lines within multiplets were measured side-on. While in this geometry the observed plasma layer is rather inhomogeneous, this is of no significance here, since lines within multiplets have practically the same upper excitation energies, so that according to Eq. (1) their A ratios are essentially temperature independent. In the second part of the experiment we selected a strong line from each multiplet and measured its intensity against a selected reference line, using the arc in the end-on configuration. In these end-on observations of the central region of the plasma, the nitrogen line emission comes from an approximately homogeneous plasma layer in the midsection of the arc, about 23 mm long. This is the part of the arc column operated in helium with a small nitrogen admixture while the areas near the electrodes are operated in argon. These measurements cover multiplets with significantly different excitation potentials for the upper states, so that emission from a well-defined, approximately homogeneous plasma layer of known temperature becomes a significant condition to obtain accurate A ratios from Eq. (1). It should be noted here that the helium plasma is quite constricted so that no bulging of the arc column is noticeable in the relatively wide spacers between the arc plates.

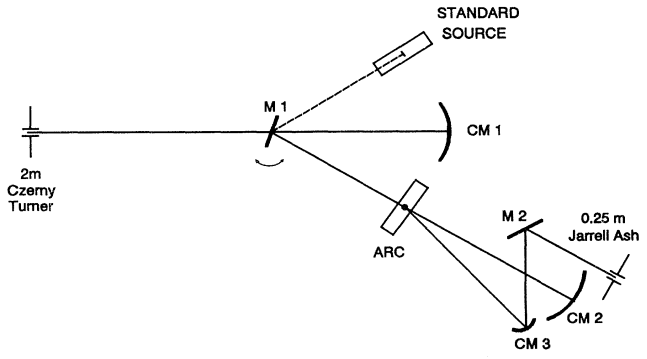

FIG. 2. Schematic optical arrangement. $M1$ and $M2$ are plane mirrors and CM1, CM2, and CM3 are concave mirrors.

The measurement setups for the side-on and end-on experiments were slightly different. In the side-on runs, the spectra were recorded on a point-by-point basis by rotating the grating of the Czerny-Turner monochromator with a stepping motor, and by measuring the intensity of the light at the exit slit with a photomultiplier. In the end-on runs, the exit slit of the monochromator was removed and the photomultiplier replaced by a charge-coupled-device (CCD) camera. Two different gratings were used for the measurements, one with 600 lines/mm blazed at 1 μm for wavelengths longer than 8000 Å and another with 1800 lines/mm for shorter wavelengths. In the case of the 600 lines/mm grating the spectral resolution was 0.36 Å and a wavelength range of 195 Å was covered by the CCD detector at the same time, while in the case of the 1800 lines/mm grating these values were 0.12 Å and 65 Å, respectively. The collection of the experimental data and the angular position of the grating were fully computer controlled. After having recorded the spectral lines, the line intensity analysis was carried out by fitting the sum of a Lorentzian and Gaussian function plus a slowly varying continuum to the obtained profiles. This superposition of functions produced excellent fits to the observed profiles, and asymmetries were found to be negligibly small. The total line intensities were then calculated by integrating the fitted Lorentzian and Gaussian functions, and finally the intensities were calibrated with a tungsten strip lamp radiation standard. All line profile measurements were repeated four times and were reproducible within 3%, and for the stronger lines within 1%.

IV. PLASMA DIAGNOSTICS

Our temperature measurements are based on the assumption that the arc plasma is in partial local thermodynamic equilibrium (partial LTE) for all atomic states with principal quantum numbers $n \geq 3$. This condition is, according to equilibrium criteria [12] as well as experimental tests [13], fulfilled for low temperature (1 eV) plas-

mas with ionization potentials similar to that of hydrogen, when the electron density is 2×10^{14} cm^{-3} or larger. Since our density is an order of magnitude above that limit, as shown below, we may assume that the N I and N II excited-state populations follow Boltzmann distributions. We thus apply the Boltzmann-plot technique [10] to determine the excitation temperature. We have utilized two sets of lines.

(a) A few N I lines arising from different energy levels with an energy spread of 1.7 eV.

(b) Some N II lines within an energy interval of 2.7 eV.

Using the N I lines (with theoretical A values [3,14]), a relatively crude temperature value of 10 000±1500 K was obtained in the side-on measurements, while using the N II lines (again with theoretical A values [14]) a temperature of 14 400±150 K was determined in both the side-on and the end-on cases. These results indicate that the radiation of N II lines originated mainly from the high-temperature layers close to the arc axis, while the cooler outer plasma layers contributed appreciably to the N I emission. We used the temperature value of 10 000 K resulting from the side-on measurements for the determination of relative transition probabilities of the individual lines within a given multiplet [see Eq. (2)]. As noted earlier, this relatively inaccurate temperature value is not critical in this case, because our measurements involved line intensities either from identical or very close lying upper levels where the energy gaps are typically 0.01 eV.

In the end-on experiment, where the observation was confined to the central part of the arc close to its axis, the much more accurate value of 14 400±150 K was obtained. The purpose of this experiment was to connect the strong lines of different multiplets with each other. The energy intervals between the upper levels of these lines are larger so that the electron temperature plays an important role here.

The electron density was measured by two independent approaches:

(1) The addition of a trace of hydrogen to the helium gas permitted a measurement of the width of the Balmer H_β line which is predominantly broadened by the interatomic Stark effect [12,15]. Applying the results of Stark broadening calculations of Vidal, Cooper, and Smith [15], electron densities in the range from 2 to 3×10^{15} cm^{-3} were obtained for the plasma layers principally contributing to the H_β line emission.

(2) A study of the complex helium lines at 4471 Å based on results of Czernichowski and Chapelle [16] yielded an electron density of 2×10^{15} cm^{-3}. We utilized both the displacement of the forbidden component to the allowed one and the intensity ratio of these two.

We note that these values for the electron density N_e, which are in excellent agreement, are far above the required limit of $N_e=2\times10^{14}$ cm^{-3} for the existence of partial LTE.

V. RESULTS AND DISCUSSION

We have measured the relative transition probabilities of about 100 spectral lines of N I with a wall-stabilized arc, and obtained an experiment-based absolute scale by normalizing the transition probabilities of the $3s\,^4P_{5/2}-3p\,^4D^o_{7/2}$ and the $3s\,^4P_{1/2,3/2,5/2}-3p\,^4S^o_{3/2}$ lines at 8680 Å and at 7468, 7442, and 7424 Å, respectively, with lifetime data available for their upper states. We applied the measurements of Bengtsson *et al.* [17], Copeland *et al.* [18], and Catherinot and Sy [19] which were

TABLE I. (a) Lifetime data obtained by the laser-induced fluorescence method used for normalization of N I emission data. (b) Decay rates in (10^8 s^{-1}) for the $3p\,^4D^o$ and $3p\,^4S^o$ levels. Our relative emission data are normalized for best fit, using the same normalization constant for both transitions.

(a)

Level	Author	Lifetime τ (ns)	Averaged τ (ns)
$3p\,^4D^o_{7/2}$	Bengtsson *et al.* [14]	44±2	43.5
	Copeland *et al.* [15]	43±3	
$3p\,^4S^o_{3/2}$	Bengtsson *et al.* [14]	26.0±1.5	24.7
	Catherinot *et al.* [16]	23.3±2.3	

(b)

		Partial decay rates into $3s\,^4P$		
Atomic level (1)	Total decay rate from τ average (2)	This expt., best fit of relative scale (3)	Theory into $2s2p^4\,^4P$ (4)	Total decay rate, sum of (3) and (4)
$3p\,^4D^o_{7/2}$	0.230	0.221	0.010	0.231
$3p\,^4S^o_{3/2}$	0.405	0.369	0.036	0.405

TABLE II. Results, including estimates of expanded uncertainties, and comparison with recent theoretical and experimental data. In the first line for each multiplet, the weighted multiplet values are given in italics.

Configuration		Term		Wavelength	Stat. Weight		Transition probability A (10^8 s^{-1})				
Lower	Upper	Lower	Upper	(Å)	g_i	g_k	This expt.	Hibbert *et al.* [3]	Burke and Lennon [1]	Weiss and Suskin [5]	Zhu *et al.* [7]
$2s^22p^2(^3P)3s$	$2s^22p^2(^3P)3p$	^4P	$^4D^o$	*8961.6*	*12*	*20*	*2.25*[−1][a]±*11%*	*2.59*[−1]	*1.83*[−1]	*2.55*[−1]	
				8680.28	6	8	2.21[−1]±11%	2.60[−1]		2.56[−1]	
				8683.40	4	6	1.67[−1]±11%	1.93[−1]		1.79[−1]	
				8686.15	2	4	1.04[−1]±11%	1.18[−1]		1.07[−1]	
				8718.84	6	6	5.95[−2]±12%	6.73[−2]		7.59[−2]	6.60[−2]
				8711.70	4	4	1.17[−1]±11%	1.32[−1]		1.35[−1]	1.26[−1]
				8703.25	2	2	1.97[−1]±11%	2.2[−1]		2.12[−1]	2.01[−1]
				8747.37	6	4	8.83[−3]±13%	9.93[−3]		1.25[−2]	1.07[−2]
				8728.90	4	2	3.24[−2]±12%	3.86[−2]		4.20[−2]	4.00[−2]
$2s^22p^2(^3P)3s$	$2s^22p^2(^3P)3p$	^4P	$^4P^o$	*8211.8*	*12*	*12*	*3.04*[−1]±*12%*	*3.14*[−1]	*2.37*[−1]	*3.13*[−1]	*3.00*[−1]
				8216.34	6	6	2.21[−1]±12%	2.31[−1]		2.19[−1]	2.04[−1]
				8210.72	4	4	5.02[−2]±12%	5.31[−2]		4.18[−2]	5.20[−2]
				8200.36	2	2	4.85[−2]±12%	4.77[−2]		5.24[−2]	5.00[−2]
				8242.39	6	4	1.34[−1]±12%	1.34[−1]		1.39[−1]	1.35[−1]
				8223.13	4	2	2.65[−1]±12%	2.67[−1]		2.60[−1]	2.54[−1]
				8184.86	4	6	7.86[−2]±12%	8.39[−2]		9.49[−2]	8.50[−2]
				8188.01	2	4	1.22[−1]±12%	1.27[−1]		1.32[−1]	1.28[−1]
$2s^22p^2(^3P)3s$	$2s^22p^2(^3P)3p$	^4P	$^4S^o$	*7452.2*	*12*	*4*	*3.69*[−1]±*11%*	*3.84*[−1]	*2.37*[−1]	*3.78*[−1]	*3.67*[−1]
				7468.31	6	4	1.90[−1]±11%	2.02[−1]		1.88[−1]	1.85[−1]
				7442.30	4	4	1.23[−1]±11%	1.24[−1]		1.27[−1]	1.20[−1]
				7423.64	2	4	5.63[−2]±11%	5.86[−2]		6.38[−2]	6.20[−2]
$2s^22p^2(^3P)3s$	$2s^22p^2(^3P)3p$	^2P	$^2D^o$	*9395.3*	*6*	*10*	*2.56*[−1]±*12%*	*2.67*[−1]	*2.66*[−1]		
				9392.79	4	6	2.55[−1]±12%	2.68[−1]			
				9386.81	2	4	2.19[−1]±12%	2.26[−1]			
				9460.68	4	4	3.88[−2]±13%	4.04[−2]			
$2s^22p^2(^3P)3s$	$2s^22p^2(^3P)3p$	^2P	$^2P^o$	*8617.5*	*6*	*6*	*2.97*[−1]±*12%*	*3.26*[−1]	*3.22*[−1]		*3.28*[−1]
				8629.24	4	4	2.52[−1]±12%	2.75[−1]			2.69[−1]
				8594.00	2	2	1.98[−1]±12%	2.16[−1]			2.31[−1]
				8655.88	4	2	9.70[−2]±12%	1.11[−1]			1.10[−1]
				8567.74	2	4	4.64[−2]±13%	5.11[−2]			5.20[−2]
$2s^2p^2(^3P)3s$	$2s^22p^2(^3P)4p$	^2P	$^2P^o$	*4666.7*	*6*	*6*	*9.72*[−3]±*14%*		1.41[−2]		
				4669.89	4	4	7.49[−3]±14%				
				4660.46	2	2	6.72[−3]±14%				
				4678.59	4	2	2.69[−3]±15%				
				4651.82	2	4	2.40[−3]±15%				
$2s^22p^2(^3P)3s$	$2s^22p^2(^1D)3p$	^2P	$^2D^o$	*4106.9*	*6*	*10*	*3.99*[−2]±*14%*	*6.76*[−2]	*2.32*[−2]		
				4109.95	4	6	3.90[−2]±14%	6.77[−2]			
				4099.94	2	4	3.48[−2]±14%	5.64[−2]			
				4113.97	4	4	6.62[−3]±14%	1.11[−2]			
$2s^22p^2(^3P)3p$	$2s^22p^2(^3P)3d$	$^2S^o$	^2P	*9049.9*	*2*	*6*	*2.91*[−1]±*13%*	*3.27*[−1]	*2.74*[−1]		
				9060.48	2	4	2.87[−1]±13%	3.27[−1]			
				9028.92	2	2	3.00[−1]±13%	3.27[−1]			
$2s^22p^2(^3P)3p$	$2s^22p^2(^3P)4d$	$^2S^o$	^2P	*6005.5*	*2*	*6*	*3.60*[−2]±*14%*		*5.13*[−2]		
				6008.47	2	4	3.58[−2]±14%				
				5999.43	2	2	3.64[−2]±14%				
$2s^22p^2(^3P)3p$	$2s^22p^2(^3P)3d$	$^4D^o$	^4F	*10116.8*	*20*	*28*	*3.66*[−1]±*13%*	*3.85*[−1]	*3.74*[−1]		
				10114.6	8	10	3.75[−1]±13%	3.91[−1]			
				10112.5	6	8	3.19[−1]±13%	3.42[−1]			

TABLE II. (*Continued*).

Configuration Lower	Configuration Upper	Term Lower	Term Upper	Wavelength (Å)	Stat. Weight g_i	Stat. Weight g_k	Transition probability A (10^8 s^{-1}) This expt.	Hibbert *et al.* [3]	Burke and Lennon [1]	Weiss and Suskin [5]	Zhu *et al.* [7]
				10 108.9	4	6	2.85[−1]±13%	3.02[−1]			
				10 105.1	2	4	2.62[−1]±13%	2.79[−1]			
				10 164.8	8	8	3.97[−2]±13%	3.99[−2]			
				10 147.3	6	6	7.31[−2]±13%	7.61[−2]			
				10 128.3	4	4	9.89[−2]±13%	9.94[−2]			
				10 200.0	8	6	3.26[−3]±14%	2.37[−3]			
				10 166.8	6	4	4.13[−3]±14%	5.79[−3]			
$2s^22p^2(^3P)3p$	$2s^22p^2(^3P)3d$	$^4D^o$	^4P	*9 988.2*	*20*	*12*	*4.34*[−2]±*13%*	*3.39*[−2]	*2.15*[−2]		
				10 054.3	8	6	1.39[−2]±13%	6.68[−3]			
				9 968.5	6	4	4.50[−3]±14%	4.83[−4]			
				9 905.5	4	2	3.11[−3]±14%	2.74[−4]			
				10 003.0	6	6	2.28[−2]±13%	2.47[−2]			
				9 931.5	4	4	3.64[−2]±13%	2.79[−2]			
				9 883.4	2	2	2.93[−2]±13%	3.00[−2]			
				9 965.7	4	6	7.60[−3]±14%	3.32[−3]			
				9 909.2	2	4	7.58[−3]±14%	7.07[−3]			
$2s^22p^2(^3P)3p$	$2s^22p^2(^3P)3d$	$^4D^o$	^4D	*9 830.6*	*20*	*20*	*8.75*[−2]±*13%*	*9.59*[−2]	*9.77*[−2]		
				9 863.33	8	8	8.82[−2]±13%	1.00[−1]			
				9 822.75	6	6	4.79[−2]±13%	4.90[−2]			
				9 798.56	4	4	2.99[−2]±13%	2.41[−2]			
				9 788.29	2	2	3.22[−2]±13%	2.64[−2]			
				9 872.15	8	6	2.58[−2]±13%	3.24[−2]			
				9 834.61	6	4	4.10[−2]±13%	4.72[−2]			
				9 810.01	4	2	4.77[−2]±13%	5.60[−2]			
				9 814.02	6	8	5.34[−3]±14%	7.51[−3]			
				9 786.78	4	6	1.09[−2]±13%	1.12[−2]			
				9 776.90	2	4	1.16[−2]±13%	1.15[−2]			
$2s^22p^2(^3P)3p$	$2s^22p^2(^3P)3d$	$^4P^o$	^4P	*10 707.2*	*12*	*12*		*1.34*[−1]	*1.17*[−1]		
				10 757.9	6	6	2.37[−2]±*13%*	3.07[−2]			
				10 673.9	4	4	[b]	2.57[−3]			
				10 623.2	2	2	3.39[−2]±13%	9.48[−2]			
				10 718.0	6	4	2.29[−2]±13%	2.74[−2]			
				10 644.0	4	2	4.01[−2]±13%	4.18[−2]			
				10 713.5	4	6	4.18[−2]±13%	1.00[−1]			
				10 653.0	2	4	5.55[−2]±13%	1.10[−1]			
$2s^22p^2(^3P)3p$	$2s^22p^2(^3P)3d$	$^4P^o$	^4D	*10 526.3*	*12*	*20*	*2.39*[−1]±*13%*	*2.47*[−1]	*2.63*[−1]		
				10 539.6	6	8	2.35[−1]±13%	2.51[−1]			
				10 507.0	4	6	1.23[−1]±13%	1.11[−1]			
				10 500.3	2	4	6.07[−2]±13%	4.25[−2]			
				10 549.6	6	6	1.13[−1]±13%	1.34[−1]			
				10 520.6	4	4	1.52[−1]±13%	1.54[−1]			
				10 513.4	2	2	1.78[−1]±13%	1.45[−1]			
				10 563.3	6	4	3.24[−2]±13%	4.33[−2]			
				10 533.8	4	2	7.16[−2]±13%	1.01[−1]			
$2s^22p^2(^3P)3p$	$2s^22p^2(^3P)5s$	$^4P^o$	^4P	*6 954.9*	*12*	*12*	*2.41*[−2]±*14%*		*2.65*[−2]		
				6 945.18	6	6	1.75[−2]±14%				
				6 960.50	4	4	4.45[−3]±15%				
				6 973.07	2	2	3.65[−3]±15%				
				6 979.18	6	4	9.37[−3]±15%				
				6 982.03	4	2	1.94[−2]±15%				
				6 926.67	4	6	7.38[−3]±15%				
				6 951.60	2	4	9.79[−3]±15%				
$2s^22p^2(^3P)3p$	$2s^22p^2(^3P)5s$	$^2D^o$	^2P	*7 546.4*	*10*	*6*	*2.29*[−2]±*14%*		*2.93*[−2]		
				7 550.91	6	4	1.79[−2]±14%				

TABLE II. (*Continued*).

Configuration Lower	Configuration Upper	Term Lower	Term Upper	Wavelength (Å)	Stat. Weight g_i	Stat. Weight g_k	Transition probability A (10^8 s^{-1}) This expt.	Hibbert *et al.* [3]	Burke and Lennon [1]	Weiss and Suskin [5]	Zhu *et al.* [7]
				7 546.21	4	2	2.85[−2]±14%				
				7 507.61	4	4	2.30[−3]±15%				
$2s^22p^2(^1D)3s$	$2s^22p^2(^1D)3p$	^2D	$^2F^o$	*9 047.6*	*10*	*14*	2.66[−1]±14%	2.73[−1]	2.86[−1]		
				9 045.88	6	8	2.63[−1]±14%	2.74[−1]			
				9 049.89	4	6	2.68[−1]±14%	2.55[−1]			
				9 049.49	6	6		1.84[−2]			
$2s^22p^2(^1D)3s$	$2s^22p^2(^1D)3p$	^2D	$^2P^o$	*7 904.5*	*10*	*6*	1.46[−1]±14%	3.82[−1]	2.46[−1]		
				7 915.42	4	2	1.48[−1]±14%	3.81[−1]			
				7 898.98	6	4	1.45[−1]±14%	3.43[−1]			
				7 899.28	4	4		3.99[−2]			
$2s^22p^2(^1D)3s$	$2s^22p^2(^1D)3p$	^2D	$^2D^o$	*9 195.7*	*10*	*10*	1.24[−1]±14%	2.61[−1]	1.42[−1]		
				9 187.45	6	6	1.28[−1]±14%	2.44[−1]			
				9 187.86	4	6		1.76[−2]			
				9 208.00	4	4	1.18[−1]±14%	2.3[−1]			
				9 207.59	6	4		2.71[−2]			
Intersystem Lines											
$2s^22p^2(^3P)3p$	$2s^22p^2(^3P)3d$	$^4D^o$	^2F	*9 997.75*	*8*	*8*	*9.20*[−3]±*14%*	*4.12*[−3]			
				10 017.82	6	6	2.26[−2]±14%	4.21[−3]			
				9 947.07	6	8	1.08[−2]±14%	5.26[−3]			
				9 980.42	4	6	8.10[−3]±14%	5.54[−3]			
$2s^22p^2(^3P)3p$	$2s^22p^2(^3P)3d$	$^4P^o$	^2F	*10 730.5*	*4*	*6*	*1.03*[−2]±*14%*	*3.98*[−3]			

[a] 2.25[−1] equals 2.25×10^{-1}.
[b] Weak line, smaller than 6[−4].

all obtained with state-selective laser excitation techniques. In order to utilize the basic relationship [20] between the lifetime τ_k of state k and the transition probabilities A_{ki} for spontaneous emission to lower states i,

$$\tau_k^{-1}=\sum_i A_{ki} \ , \tag{6}$$

we need to include in the transition probability sum all allowed transitions into lower atomic states i. For the two upper levels involved, the sums indeed consist of several transitions, i.e., in addition to the above listed strong transitions measured by us, weak infrared transitions occur into the $2s2p^4\ ^4P$ levels. We were unable to measure these very weak transitions at 14 757 and 11 600 Å and could only determine upper limits. Richter [21] has measured the $2s2p^4\ ^4P-2s^22p^2\,3p^4S^o$ transition at 11 600 Å and obtained $A=0.041\times10^8$ s^{-1}. Weiss and Suskin [5] have calculated the A values for both transitions, and their results are used to correlate the lifetime and relative transition probability measurements. Richter's measurement and our "upper limit" determinations—as well as calculations by Hibbert *et al.* [3]—are all consistent with the Weiss and Suskin data.

We present the pertinent data for the scale normalization in Table I. For the two decay rates, we have obtained normalization factors that differ by only 0.3%, indicating the excellent consistency of the applied lifetime data. Furthermore, it is seen that the weak infrared transitions contribute only 4% and 9%, respectively, to the total decay rates, and have therefore only a small influence on the normalization procedure.

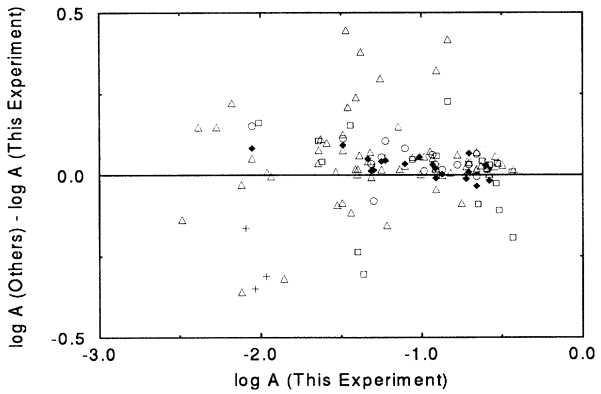

FIG. 3. Comparison of our experimental transition probability data with the results of the emission experiment by Zhu *et al.* [7] (solid diamonds); the calculations by Burke and Lennon [1] (open squares, multiplet data only); calculations by Hibbert *et al.* [3] (open triangles) and by Weiss and Suskin [5] (open circles). Shown separately are three intersystem line comparisons with Hibbert *et al.* [3] (crosses). A few large disagreements for weak lines are outside the range presented here. (The logarithms are to the base 10.)

TABLE III. Relative line strengths S in multiplets, and comparisons with the intermediate coupling (IC) data of Hibbert *et al.* and *LS*-coupling data. In each multiplet, the sum of the line strengths is set equal to 100.

Multiplet	λ (Å)	S (Expt.)	S(IC)/S(Expt.)	$S(LS)/S$(Expt.)
$3s\ ^4P-3p\ ^4D^o$	8 680.28	39.0	1.02	1.03
	8 683.40	22.2	1.00	0.95
	8 686.15	9.2	0.99	0.90
	8 718.84	8.0	0.98	1.13
	8 711.70	10.5	0.97	1.02
	8 703.25	8.8	0.98	0.94
	8 747.37	0.80	1.0	1.25
	8 728.90	1.45	1.03	1.17
$3s\ ^4P-3p\ ^4P^o$	8 216.34	36.4	1.01	0.96
	8 210.72	5.5	1.02	0.81
	8 200.36	2.7	0.95	1.05
	8 242.39	14.9	0.97	1.01
	8 223.13	14.5	0.98	0.96
	8 184.86	12.8	1.03	1.18
	8 188.01	13.2	1.02	1.05
$3s\ ^4P-3p\ ^4S^o$	7 468.31	51.7	1.02	0.97
	7 442.30	33.1	0.97	1.01
	7 423.64	15.0	1.01	1.11
$3s\ ^2P-3p\ ^2D^o$	9 392.79	59.7	1.01	1.01
	9 386.81	34.0	1.00	0.98
	9 460.68	6.17	1.00	1.08
$3s\ ^2P-3p\ ^2P^o$	8 629.24	56.7	0.99	0.98
	8 594.00	22.0	0.99	1.00
	8 655.88	11.0	1.05	1.01
	8 567.74	10.2	1.00	1.09
$3s\ ^2P-3p'\ ^2D^o$	4 109.95	58.5	1.03	1.03
	4 099.94	34.5	0.96	0.97
	4 113.97	6.65	0.99	1.00
$3p\ ^2S^o-3d\ ^2P$	9 060.48	65.9	1.02	1.01
	9 028.92	34.1	0.97	0.98
$3p\ ^4D^o-3d\ ^4F$	10 114.6	36.6	0.99	0.98
	10 112.5	24.8	1.02	0.99
	10 108.9	16.6	1.01	0.97
	10 105.1	10.2	1.01	0.98
	10 164.8	3.1	0.97	1.32
	10 147.3	4.3	1.00	1.20
	10 128.3	3.9	0.95	1.03
	10 200.0	0.20	0.69	1.05
	10 166.8	0.16	1.34	1.75
$3p\ ^4D^o-3d\ ^4P$	10 054.3	16.4	0.62	2.43
	9 968.5	3.4	0.15	6.15
	9 905.5	1.2	0.08	6.92
	10 003.0	26.3	1.39	0.34
	9 931.5	27.5	0.98	0.39
	9 883.4	10.9	1.31	0.76

TABLE III. (*Continued*).

Multiplet	λ (Å)	S (Expt.)	S(IC)/S(Expt.)	$S(LC)/S$(Expt.)
	9 965.7	8.7	0.56	0.12
	9 909.2	5.7	1.19	0.30
$3p\ ^4D^o$–$3d\ ^4D$	9 863.33	40.7	1.04	0.84
	9 822.75	16.3	0.94	1.06
	9 798.56	6.8	0.74	1.18
	9 788.29	3.6	0.75	1.39
	9 872.15	9.0	1.14	0.63
	9 834.61	9.4	1.04	0.74
	9 810.01	5.4	1.07	0.93
	9 814.02	2.4	1.29	2.38
	9 786.78	3.7	0.92	1.89
	9 776.90	2.6	0.92	1.92
$3p\ ^4P^o$–$3d\ ^4P$	10 757.9	17.0	0.68	2.06
	10 673.9	[a]		
	10 623.2	7.8	1.47	0.36
	10 718.0	10.8	0.63	1.39
	10 644.0	9.3	0.55	1.48
	10 713.5	29.5	1.27	0.51
	10 653.0	25.6	1.05	0.54
$3p\ ^4P^o$–$3d\ ^4D$	10 539.6	39.6	1.03	1.01
	10 507.0	15.3	0.88	1.37
	10 500.3	5.1	0.67	1.63
	10 549.6	14.3	1.15	0.63
	10 520.6	12.7	0.98	0.84
	10 513.4	7.4	0.86	1.12
	10 563.3	2.7	1.37	0.37
	10 533.8	3.0	1.37	0.57

[a]Very weak.

The lifetime data carry uncertainty estimates in the range from 5% to 10%. Using these estimates, as well as the excellent consistency of all four lifetime data and the almost perfect consistency of the two normalization factors, we estimate the absolute scale to have a standard uncertainty of ±5%. Our data are on average a few percent smaller than those of the emission experiment of Zhu *et al.* [7], who used the same normalization technique but without the lifetime data of Bengtsson *et al.* [17] which were not available to them.

Table II contains all our measured data, plus the derived multiplet values, on this absolute scale. In addition, we list the recent theoretical data by Weiss and Suskin [5], Hibbert *et al.* [3], and the Opacity Project data [1] (which are multiplet data only), and the experimental data of Zhu *et al.* [7] for comparison.

A graphical comparison is given in Fig. 3. The agreement with the data of Zhu *et al.*, which are limited to $3s$-$3p$ transitions but are obtained by a similar stabilized-arc emission experiment, is typically at the ±10% level, but the agreement with the calculated data varies a great deal. The scatter between the data increases for the weaker lines, as expected.

In Table III, we compare—separately for each multiplet—our relative line strength measurements, normalized to a total multiplet strength $S_M = 100$, with the intermediate coupling data of Hibbert *et al.* [3] and with the *LS*-coupling predictions.

Several observations may be made. (a) For $3s$-$3p$ multiplets, the experiments indicate that the departures from *LS* coupling are within the estimated experimental uncertainties or are only slightly larger. (This is also indicated by the intermediate coupling calculations.) (b) For $3p$-$3d$ transitions, the departures of our measurements from *LS* coupling become larger, especially for the weaker lines; but here again the intermediate coupling calculations are in better agreement with experiment. (c) Even when considerable differences between experiment and *LS* coupling exist for weaker lines, disagreements for the strong lines are often much smaller.

The uncertainties listed for the transition probabilities in Table II have been estimated by taking into account the following contributions—all given as standard uncertainties:

(a) Standard deviations of the mean values of the line intensity measurements, typically in the range from

±1%–±3%, determined separately for each line.

(b) Systematic uncertainties of the line profile fitting procedure, approximately ±2%.

(c) Uncertainties in the treatment of self-absorption, ±2% or less.

(d) Uncertainties in the temperature determination (these depend on the excitation energy of each line relative to the lines used for the scale normalization, and range from 0 to ±2%).

(e) Uncertainties due to plasma layer averaging in both side-on and end-on observations, estimated to be up to ±3% between multiplets, depending on the differences in excitation energies.

(f) Uncertainties in the radiometric calibration procedure, from 0% to 2%, depending on the wavelength positions relative to the reference lines.

(g) Possible deviations from linearity of the photoelectric detection system, estimated to be less than 1%.

(h) Uncertainties in the lifetime data and in the applied A values of the weak $2s2p^4\ ^4P-2s^22p^23p\ ^4D^o, ^4S^o$ transitions, required for the absolute scale of the transition probability data; these are estimated to be ±5%.

The combined uncertainties, treated as the root of the sum of the squares (RSS) of the individual uncertainty contributions, lie in the range from ±5.5% to ±7.5%. The expanded uncertainties, defined as twice the RSS, are given in Table II.

Our data are thus fully consistent with the experimental data of Zhu *et al.* (their estimated uncertainties are in the range of ±12–15 %), and are in most cases in good agreement with the calculated data of Hibbert *et al.*, Weiss and Suskin, and Burke and Lennon, considering that the uncertainties of the calculations are also estimated to be in the 10–20 % range. The larger disagreements of this experiment with the calculations for some $3p$-$3d$ transitions as well as for the intersystem lines are expected to be mainly due to problems in the treatment of electron correlation and relativistic corrections in the calculations. The electron-correlation effects appear to be especially large when either the ^2P or ^4P levels are involved because of near coincidences in the excitation energies for $3d\ ^2P$ and $4s\ ^2P$, as well as $3d\ ^4P$ and $4s\ ^4P$. (Analogous situations are found for $4d\ ^2P, ^4P$ and $5s\ ^2P, ^4P$, etc.) It should be emphasized that our experimental results are of similar quality for all measured lines—with a slight deterioration for the weaker intersystem lines—since the same technique is applied throughout.

ACKNOWLEDGMENTS

J.M. was supported in part by the M. Sklodowska-Curie Foundation and G.V. had partial support from the U.S.–Hungarian Joint Fund.

[1] V. M. Burke and D. J. Lennon (unpublished).
[2] K. A. Berrington, P. G. Burke, K. Butler, M. J. Seaton, P. J. Storey, K. T. Taylor, and Yu Yan, J. Phys. B **20**, 6379 (1987).
[3] A. Hibbert, E. Biemont, M. Godefroid, and N. Vaeck, Astron. Astrophys. Suppl. Ser. **88**, 505 (1991).
[4] A. Hibbert, Comput. Phys. Commun. **9**, 141 (1975).
[5] A. W. Weiss and M. Suskin (unpublished).
[6] C. Goldbach, T. Lüdtke, M. Martin, and G. Nollez, Astron. Astrophys. **266**, 605 (1992).
[7] Q. Zhu, J. M. Bridges, T. Hahn, and W. L. Wiese, Phys. Rev. A **40**, 3721 (1989).
[8] C. E. Moore, *Table of Spectra of Hydrogen, Carbon, Nitrogen and Oxygen Atoms and Ions,* edited by J. Gallagher (CRC, Boca Raton, FL, 1993).
[9] W. L. Wiese, M. W. Smith, and B. M. Glennon, *Atomic Transition Probabilities—Hydrogen through Neon,* Natl. Bur. Stand. Ref. Data Ser., Nat. Bur. Stand. (U.S.) Circ. No. 4 (U.S. GPO, Washington, DC, 1966), Vol. I (see general introduction).
[10] W. L. Wiese, in *Methods of Experimental Physics,* edited by B. Bederson and W. L. Fite (Academic, New York, 1968), Vol. 7B, pp. 307–353.
[11] V. Helbig, D. E. Kelleher, and W. L. Wiese, Phys. Rev. A **14**, 1082 (1976).
[12] H. R. Griem, *Plasma Spectroscopy* (McGraw-Hill, New York, 1964).
[13] J. B. Shumaker and C. H. Popenoe, J. Res. Natl. Bur. Stand. **76A**, 71 (1972).
[14] D. Luo and A. K. Pradhan, J. Phys. B **22**, 3377 (1989).
[15] C. R. Vidal, J. Cooper, and E. W. Smith, Astrophys. J. Suppl. Ser. **25**, 37 (1973).
[16] A. Czernichowski and J. Chapelle, J. Quant. Spectrosc. Radiat. Transfer **33**, 427 (1985).
[17] G. J. Bengtsson, J. Larsson, S. Svanberg, and D. D. Wang, Phys. Rev. A **45**, 2712 (1992).
[18] R. A. Copeland, J. B. Jeffries, A. P. Hickman, and D. R. Crossley, J. Chem. Phys. **86**, 4876 (1987).
[19] A. Catherinot and A. Sy, Phys. Rev. A **20**, 1511 (1979).
[20] W. L. Wiese, in *Progress in Atomic Spectroscopy, Part B,* edited by W. Hanle and H. Kleinpoppen (Plenum, New York, 1979).
[21] J. Richter, Z. Astrophys. **51**, 177 (1961).